Progress In Electromagnetics Research M, Vol. 107, 243–257, 2022

Optimizing Turn-on Angle and External Rotor Pole Shape to Suppress Torque Ripple of a Novel Switched Reluctance Motor

Chaozhi Huang, Jinfeng Duan*, Wei Liu, and Yuliang Wu

Abstract—The large vibration and noise of switched reluctance motor (SRM) limits development in the field of electric bicycles. The innovation of the paper lies in reducing torque ripple by advancing the turn-on angle and increasing air-gap permeability in the first half of two phase exchange region. The torque ripple of a novel Multi-Teeth External Rotor SRM (MTER-SRM) is studied in the paper. Firstly, the topology structure, working principle, and optimized process of the MTER-SRM are introduced. Secondly, the method to suppress the torque ripple by advancing turn-on angle is proved theoretically. The effect of advancing turn-on angle on torque ripple is analyzed, and turn-on angle is optimized by Finite Element Method (FEM). Thirdly, the mathematical model is built to analyze the change of air-gap permeability in the aligned and unaligned position. The effect of different angles and heights of pole shoe on the torque characteristics is analyzed by FEM, and optimized parameters of single pole shoe size are obtained. Finally, the results show that torque ripple has dropped from 1.5 to 0.4, with the decrease of 73.3%. The multi-physical field results show that the vibration displacement, velocity, acceleration, and noise pressure of stator decrease by 83.3%, 52.5%, 52.2%, and 54.2%, respectively. Meanwhile, the vibration test of the prototype also shows that the maximum vibration acceleration has dropped from 0.4 to 0.1, with the decrease of 75%. The vibration and noise of the MTER-SRM is decreased significantly by this method, which can provide a demonstration for developing high performance motor applied in electric bicycle.

1. INTRODUCTION

The SRM has been applied and popularized in many fields because of its the simple structure, high starting torque, and high reliability. However, it produces large vibration and noise in the running, which limits the development in some fields, such as electric bicycles [1, 2].

Many literatures show that the torque ripple, resulting from the exchanging of two phase current, can cause large vibration and noise, so it is very important to restrain torque ripple in order to decrease vibration and noise [3, 4]. Andrada et al. embedded PMs in stator teeth, thus significantly reducing the torque ripple and cogging torque [5]. Jeong and Lee designed a rotor pole of S12-R8 as an independent fan structure, which improve the inductance and magnetic flux at the unaligned position, and results show that average torque is improved, but the torque ripple is larger [6]. On the basis of the S8-R6, Mousavi-Aghdam et al. optimized the stator pole shoe arc of the conventional SRM to obtain nonuniform air-gap to reduce torque ripple [7]. Gundogmus et al. proposed that slots on the teeth top of the stator and rotor can change part of the radial magnetic density into tangential to reduce radial force wave. In addition, the slot can also buffer the radial force and effectively suppress the vibration and noise [8]. Lee et al. obtained a uniform air-gap between the stator and rotor at the aligned position by changing the rotor teeth shape, and then obtained an asymmetrical inductance curve. Experiments show that the machine has low torque ripple, and it is concluded that torque ripple of external rotor with single

Received 30 October 2021, Accepted 24 January 2022, Scheduled 4 February 2022
* Corresponding author: Jinfeng Duan (jinfeng_wind@163.com).
The authors are with the School of Electrical and Automation, Jiangxi University of Science and Technology, Ganzhou, China.

pole shoe is lower [9]. Jiang et al. optimized the key parameters of the S24-R16 Hybrid Reluctance Motor (HRM) by multi-objective and concluded that the single pole shoe of the stator can effectively reduce the torque ripple [10]. Single pole shoes were added at the top of stator teeth, which reduced the torque ripple. On the basis of that, the radial force was suppressed by setting a rectangular slot at the top of the stator teeth [11]. Lee obtained the ideal torque density by modifying the rotor pole shoe shape, thus reducing torque ripple [12]. Yang et al. studied the effect of stator and rotor helical teeth on vibration and noise [13]. Nabeta et al. studied the effect of special rotor shape on the vibration and torque ripple suppression of SRM [14]. Guo et al. proposed a method to select the best turn-on angle based on efficiency to reduce the amplitude of the third harmonic current and the sixth radial force harmonic, so as to reduce resonance [15]. Li et al. and Lee et al. made triangular slots on one side of the rotor. The results showed that the maximum torque difference was reduced, which effectively reduced the torque ripple [16, 17]. Zhang et al. suggested setting rectangular slots on both sides of rotor teeth to change air-gap magnetic density in the aligned position to reduce the torque ripple [18, 19]. Lin and Yang, and Mousavi-Aghdam et al. proposed a new structure MTER-SRM based on the method of energy conversion efficiency, and it had lower torque ripple than the conventional SRM [20, 21].

A method that the torque ripple is restrained by varying turn-on angle and adding single pole shoe is put forward in this paper based on a new structure of MTER-SRM applied in the field of electric bicycles proposed by [21]. Firstly, the operating principle of the motor is introduced in the paper. Secondly, the effect of varying angle of turn-on and the size of single shoe on the torque ripple is analyzed. Thirdly, the torque characteristics at different turn-on angles and sizes of pole shoe are analyzed by FEM. Finally, prototype experiments show that the torque ripple of the optimized model is lower, and vibration and noise are effectively reduced.

2. WORKING PRINCIPLE AND OPTIMIZED PROCESS

2.1. Topology Structure and Working Principle

Fig. 1 shows the topology structure of MTER-SRM. The motor consists of 6 W-type stator blocks with concentrated winding and radially opposite windings connected in series as one phase. There are 24 stator teeth and 22 rotor teeth in the motor. Table 1 displays the main parameters of the machine.

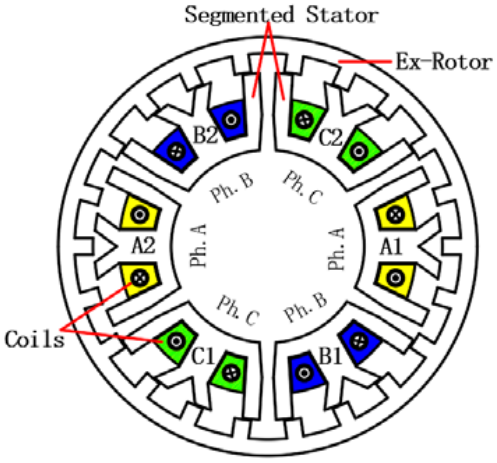

Figure 1. The geometric model MTER-SRM.

The MTER-SRM follows the principle of minimum reluctance. The position of rotor is unaligned completely with stator of ph. A, as shown in Fig. 2(a), which is defined as the initial position of the external rotor. When ph. A is excited, the magnetic flux is divided into 2 parts which pass through the air-gap respectively, and then return to the stator tooth through the air-gap again. The external rotor rotates from the initial position to position where the position of rotor is unaligned completely with stator of ph. B, as shown in Fig. 2(b). The current of ph. B is excited again; and the current of ph. A

Table 1. The parameters of MTER-SRM.

Items	Size	Items	Size
Stator outer diameter (mm)	142.28	Rotor outer diameter (mm)	172
Stator inner diameter (mm)	79.28	Rotor inner diameter (mm)	143.48
Stator yoke thickness (mm)	6.83	Rotor yoke thickness (mm)	6.76
Stator tooth width (mm)	24.8	Rotor tooth width (mm)	7.51
Stator pole shoe arc (°)	5.58	Rotor pole shoe arc (°)	5.46
Air-gap length (mm)	0.6	Axial length (mm)	100
Number of coil turns per pole shoe	55	Copper space factor	65.4%

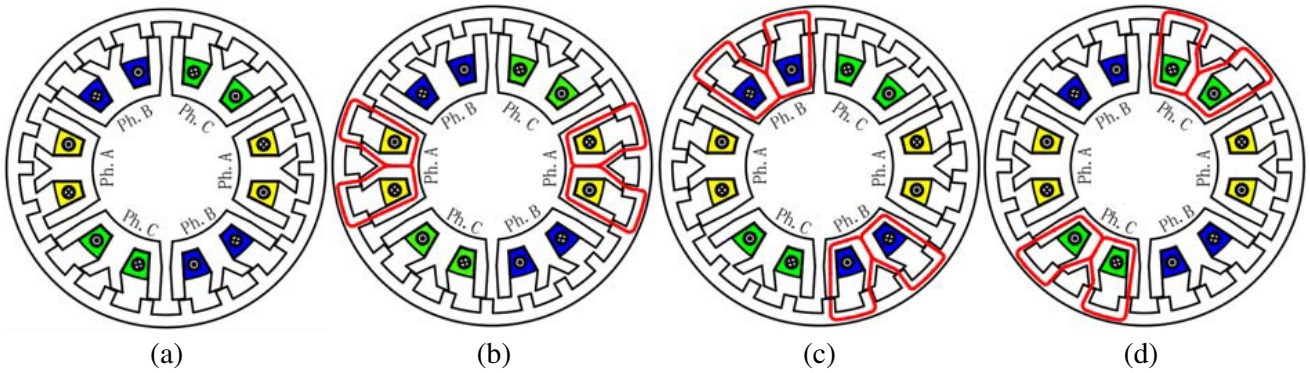

Figure 2. The operating principle of the MTER-SRM. (a) Initial position, (b) Ph. A is excited, (c) Ph. B is excited, (d) Ph. C is excited.

turns off; the rotor rotates counterclockwise to the position shown in Fig. 2(c). Similarly, the current of ph. C is excited, and the rotor rotates to the position shown in Fig. 2(d). When the three-phase windings take turns on electricity, the external rotor will keep rotating counterclockwise.

2.2. Optimize Process

The suppression of torque ripple of the motor is studied in the paper, and Fig. 3 shows its optimized process. Firstly, the angle of turn-on is optimized, and its optimal parameters get within the range. Then, the angle and height of single pole shoe are optimized, and its optimal parameters get within the range. Secondly, the harmonic response analysis and noise prediction of the optimized model are carried out. Thirdly, two prototypes are made, and the vibration test experiment is conducted.

3. PRINCIPLE OF SUPPRESSING TORQUE RIPPLE

3.1. The Effect of Advancing Turn-on on Decreasing Torque Ripple

The torque ripple of SRM can be expressed as:

$$T_{\text{rip}} = \frac{T_{\max} - T_{\min}}{T_{\text{ave}}} \times 100\% \tag{1}$$

From Equation (1), it can be seen that the minimum torque change has great influence on the torque ripple. As shown in Fig. 4, minimum torque occurs in the first half of the commutation interval (θ_{on}, θ_{overlap}). The minimum torque is at point a and low when turn-on angle is θ_{on}. The former current is not turned off yet, and the latter current rises rapidly when turn-on angle is θ'_{on}. The minimum

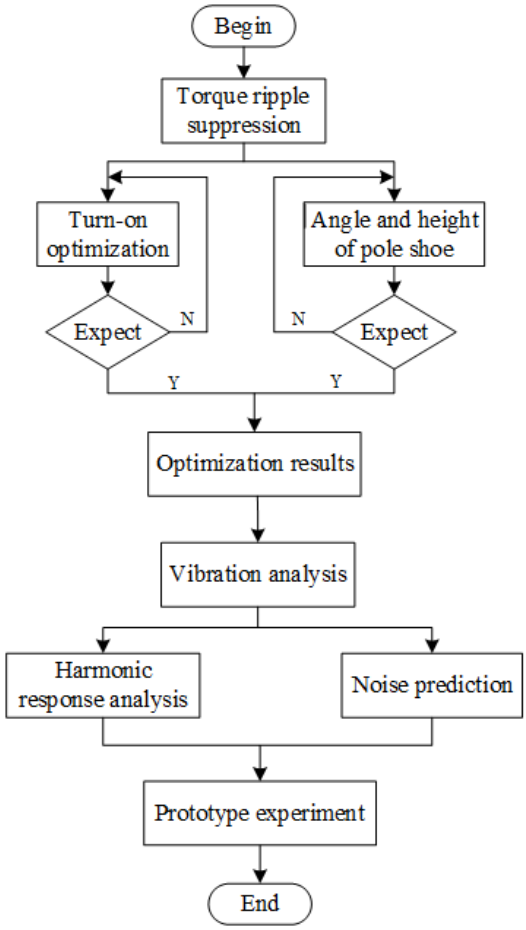

Figure 3. The flow-diagram of optimized process.

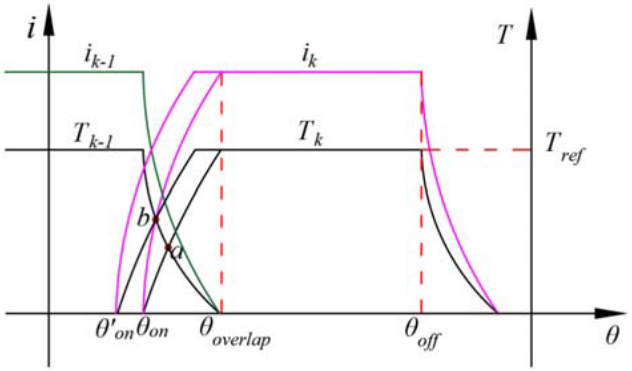

Figure 4. The torque and current characteristics with rotor angle.

torque moves forward from point a to b, which is obviously higher than point a. The minimum torque rises, and torque ripple decreases.

3.2. Electromagnetic Principle of Adding Single Pole Shoe

Changing the air-gap magnetic flux at the aligned position has great impact on the torque characteristics. Ideally, the one phase magnetic flux ψ can be expressed as:

$$\psi = Li = \left(N^2 P\right) i = \left(N^2 i\right) P \tag{2}$$

In Equation (2), where L, P, N, and i are winding inductance, permeability, coil turns, and excitation current, respectively. When N and i are constant, P is positively correlated with L and ψ. Single pole shoe makes the external rotor pole shoe coincide with stator pole shoe earlier, thus improving air-gap magnetic flux in the overlapping area.

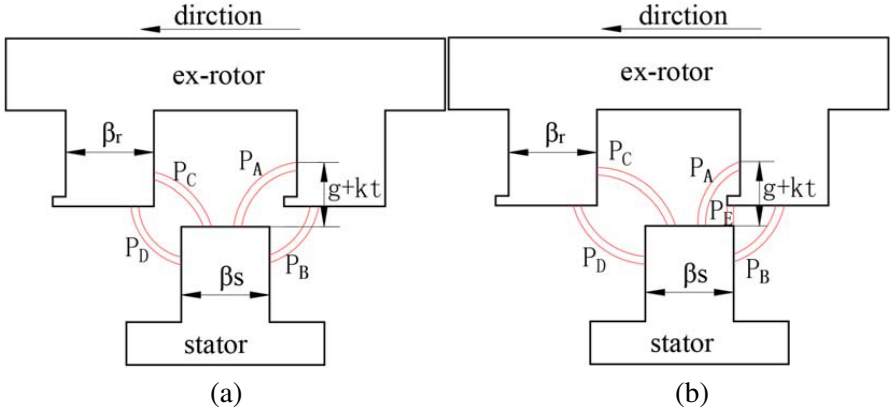

Figure 5. The magnetic divisions on air-gap. (a) Unaligned position, (b) aligned position.

For the convenience of theoretical analysis, as shown in Fig. 5. Firstly, three positions are determined: (1) external rotor pole shoe does not overlap with the stator teeth; (2) external pole shoe pole shoe partially overlaps with stator teeth; (3) external rotor pole shoe completely overlaps with stator teeth. Then, the permeance in the unaligned position is classified into P_A, P_B, P_C, and P_D, and those in the aligned position are classified into P_A, P_B, P_C, P_D, and P_E, where $P_A = P_B$ and $P_C = P_D$. Here, the initial model is briefly analyzed. The permeability analysis is as follows [20]:

$$k = \frac{t}{g+t} = \frac{r\,|\beta|}{g + r\,|\beta|} \tag{3}$$

In Equation (3), where β, g, t, and r are the external rotor rotation angle, air-gap length, external rotor rotation arc, and stator inner diameter, respectively. The average length of the magnetic circuit l is obtained by using the average approximation of the major and minor axis of ellipse.

$$l = \frac{\pi}{4}(t + g + kt) = \frac{\pi}{4}[g + (1+k)\,t] \tag{4}$$

The cross-sectional area of the area is expressed as:

$$ds = \frac{l_{stk}(dt + kdt)}{2} = \frac{l_{stk}\,(1+k)\,dt}{2} \tag{5}$$

$$dP = \frac{\mu_0 \times ds}{l} = \frac{2\mu_0 l_{stk}}{\pi} \times \frac{g + 2t}{g^2 + 2gt + 2t^2}\,dt \tag{6}$$

In Equations (5)–(6), dP and l_{stk} are permeability differential and axial length of core, respectively. The magnetic permeability of the external rotor without single pole shoe can be expressed as:

$$\begin{cases} P_A = P_B = \displaystyle\int_{r\left[\left(\frac{\pi}{22} - \frac{\beta_r + \beta_s}{2}\right) - \beta\right]}^{r\beta_r} dP \\ P_C = P_D = \displaystyle\int_{r\left[\left(\frac{\pi}{22} - \frac{\beta_r + \beta_s}{2}\right) + \beta\right]}^{r\beta_r} dP \end{cases} \tag{7}$$

The total permeability of the region is expressed as:

$$P = P_A + P_B + P_C + P_D = 2P_A + 2P_B \tag{8}$$

The magnetic permeability of external rotor with single pole shoe, and stator and rotor pole shoes are completely overlap with each other, namely $\beta \le \pi/22 - (\beta_r + \beta_s)/2 - \beta_{\text{shoe}}$.

$$\begin{cases} P_{A11} = P_{B11} = \displaystyle\int_{r\left(\frac{\pi}{22} - \frac{\beta_r+\beta_s}{2} - \beta_{\text{shoe}} - \beta\right)}^{r\beta_r} dP \\ P_{C11} = P_{D11} = P_C = P_D \end{cases} \tag{9}$$

In Equation (9), β_{shoe} is the pole shoe arc.

The total permeability of the region is expressed as:

$$P_{11} = P_{A11} + P_{B11} + P_{C11} + P_{D11} = 2P_C + 2P_{A11} \tag{10}$$

$$P_{11} - P = 2\int_{r\left[\left(\frac{\pi}{6} - \frac{\beta_r+\beta_s}{2}\right) - \beta - \beta_{\text{shoe}}\right]}^{r\left[\left(\frac{\pi}{6} - \frac{\beta_r+\beta_s}{2}\right) - \beta\right]} dP > 0 \tag{11}$$

The magnetic permeability of external rotor with single pole shoe, and stator and rotor pole shoes are partially overlap with each other, namely $\frac{\pi}{22} - \frac{\beta_r+\beta_s}{2} > \beta > \frac{\pi}{22} - \frac{\beta_r+\beta_s}{2} - \beta_{\text{shoe}}$.

$$\begin{cases} P_{A12} = P_{B12} = \displaystyle\int_0^{r\beta_r} dP \\ P_C = P_{C12} = P_{D12} = \displaystyle\int_{r\left(\frac{\pi}{22} - \frac{\beta_e+\beta_s}{2} + \beta\right)}^{r\beta_r} dP \end{cases} \tag{12}$$

$$P_E = \frac{\mu_0 l_{stk}\left[\beta + \beta_{\text{shoe}} - \left(\dfrac{\pi}{22} - \dfrac{\beta_r+\beta_s}{2}\right)\right]}{g} \cdot \frac{\beta_r+\beta_s}{2} \tag{13}$$

The total permeability of the region is expressed as:

$$P_{12} = P_{A12} + P_{B12} + P_{C12} + P_{D12} + P_E \tag{14}$$

$$P_{12} - P_{11} = 2\int_0^{r\left(\frac{\pi}{22} - \frac{\beta_r+\beta_s}{2} - \beta_{\text{shoe}} - \beta\right)} dP + P_E > 0 \tag{15}$$

It can be seen from Equations (14)–(15) that the air-gap permeability of external rotor with single pole shoe is larger than that of the initial model, so single pole shoe can effectively improve the air-gap permeability in the aligned and unaligned position. Thus, increasing air-gap magnetic flux can increase minimum torque and reduce the torque ripple.

4. OPTIMIZED EXPERIMENT OF REDUCING TORQUE RIPPLE

4.1. Optimized Experiment of Advancing Turn-on Angle

As shown in Fig. 1, the rotor pole pitch is 180/11°, and the current conduction angle of single-phase wingdings is 60/11°, because the MTER-SRM has 22 rotor teeth. The machine runs at the mode of current chopping control (CCC). The turn-on angle is stepped from 0° to −2° by 0.5°, and the models with different turn-on angles of turn-on are simulated by the FEM.

As can be seen from Fig. 6, no matter whether the turn-on angle is 0° or −1.5°, maximum torque is always around 29 N·m, but the minimum torque varies greatly. The exchanging points of ph. A and ph. B are at point a and point b respectively when the turn-on angle is 0° or −1.5°, and the corresponding minimum torques are 5.6 N·m and 8.1 N·m, respectively. Because ph. B current reaches ahead the chopping value when the turn-on angle is −1.5°, the changing point moves forward from point a to point b. According to Equation (1), the minimum torque is increased.

As shown in Fig. 7, average torque increases from 16.5 N·m to 17.3 N·m when the turn-on angle varies from 0° to −1.5°, and torque ripple decreases from 1.5 to 1.2, with the decrease of 20%. The torque characteristics are better when turn-on angle is −1.5°, where the average torque is the largest

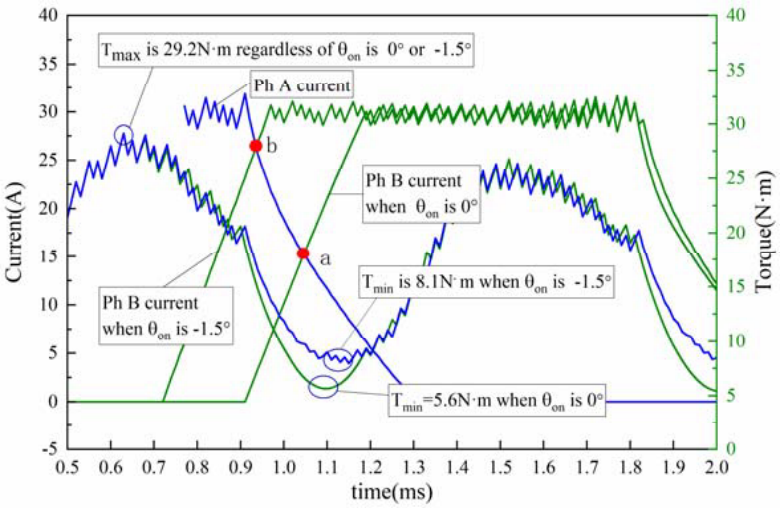

Figure 6. The current and torque of turn-on angle advance.

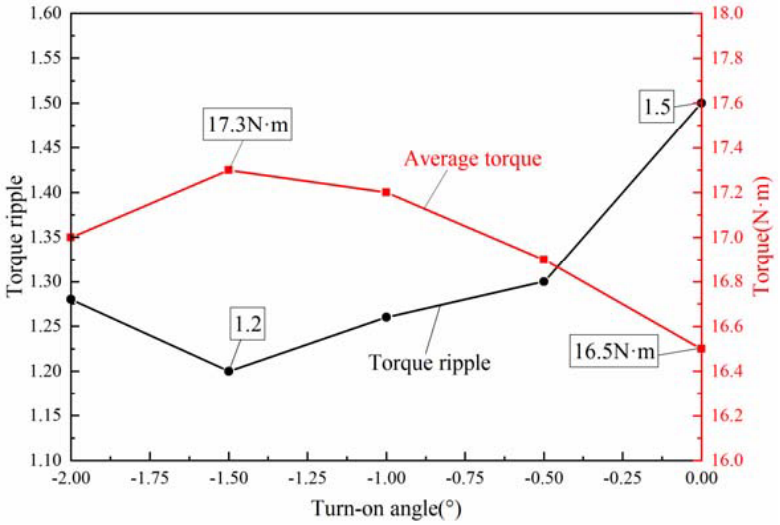

Figure 7. The torque characteristics of turn-on angle advance.

and torque ripple the lowest. The average torque decreases, and torque ripple increases when the turn-on angle is $-2°$. The reason is that the ph. A current is in the chopping stage, and ph. B current rises rapidly when the rotor of ph. B is still near the completely unaligned position with the lower inductance change rate, leading to less torque, therefore reducing the minimum torque and increasing the torque ripple. The optimal turn-on angle is selected as $-1.5°$.

4.2. Optimized Experiment of Adding Single Pole Shoe

A single pole shoe is added at the side of the external rotor in order to decrease the torque ripple, as shown in Fig. 8.

Taken ph. A and ph. B as an example, an electrical period is divided into 3 regions: M, N, and P, as shown in Fig. 9. Region Q which is similar to M is the first region in the second electrical period.

Region M is between θ_{on} where the current of ph. B starts to rise and θ_{Ta} where the current of ph. A is turned off. The inductance change rate of ph. A begins to decrease in this region, and the larger the angle of pole shoe is, the smaller the inductance change rate is, and the smaller the torque of ph. A

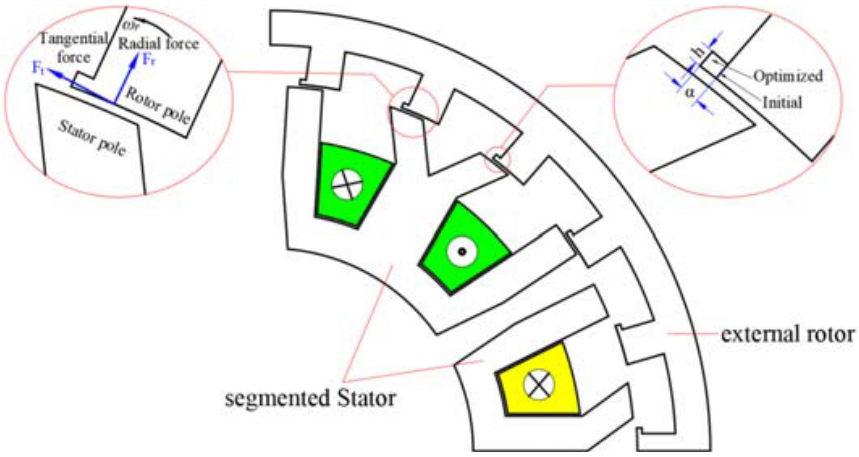

Figure 8. Single pole shoe of ex-rotor.

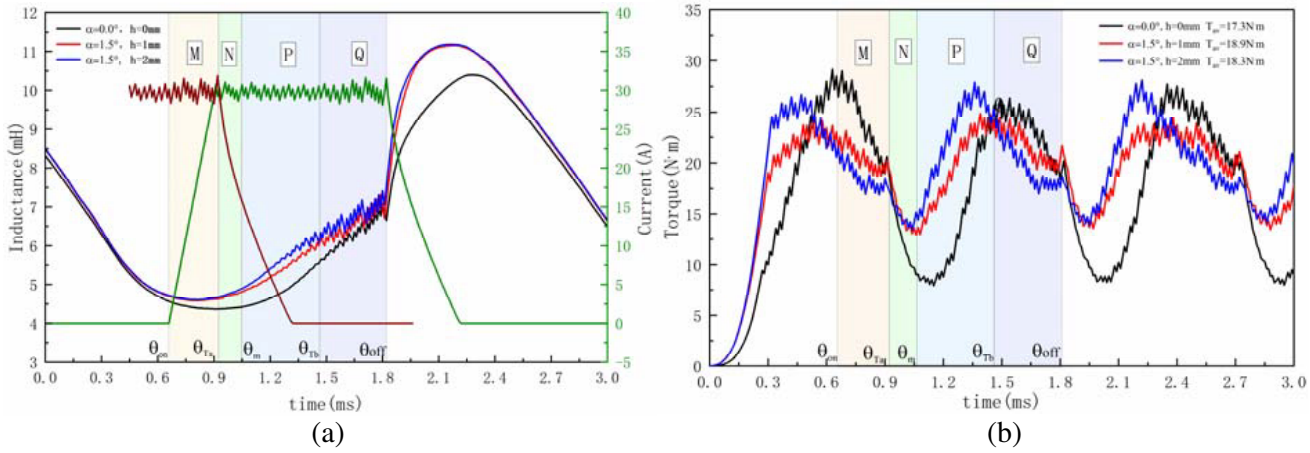

(a) (b)

Figure 9. Torque and inductance of different pole shoe sizes. (a) Inductance, (b) torque.

is. In addition, the torque generated by ph. B is low, which makes the synthesis torque continuously decrease.

There exists an N region, which starts at the point where the current of ph. A is turned off and ends at the point where the inductance of phase begins to increase rapidly. The torque of ph. A decreases rapidly, and the torque of ph. B is still small in this region, which makes synthetic torque reach minimum at θ_m.

P region is between the point θ_m and point θ_{Tb} where the synthetic torque reaches the peak. The current of ph. B is in the chopping state in this region. The external rotor teeth without single pole shoe cannot overlap with the stator teeth, so the inductance change rate is almost zero. However, the external rotor teeth with single pole shoe have already overlapped with stator teeth where the inductance change rate begins to change rapidly. The minimum inductance increases with the increase of pole shoe height.

The size of pole shoe has obvious effects on torque characteristics. As shown in Fig. 10, the average torque and torque ripple of the external rotor without single pole shoe are 17.3 N·m and 1.2, respectively. The average torque increases slightly when a single pole shoe is added at the side of external rotor teeth. The air-gap magnetic flux increases in the overlapping region, which makes the minimum torque increase. No matter how the size of pole shoe changes, the average torque remains almost at 18.5 N·m. However, the torque ripple decreases more obviously with the increase of pole shoe angle, so 2° is selected as the optimal angle of pole shoe. The torque ripple decreases with the increase of pole shoe height, and it reaches the minimum when the height of pole shoe is 1.5 mm, so 1.5 mm is

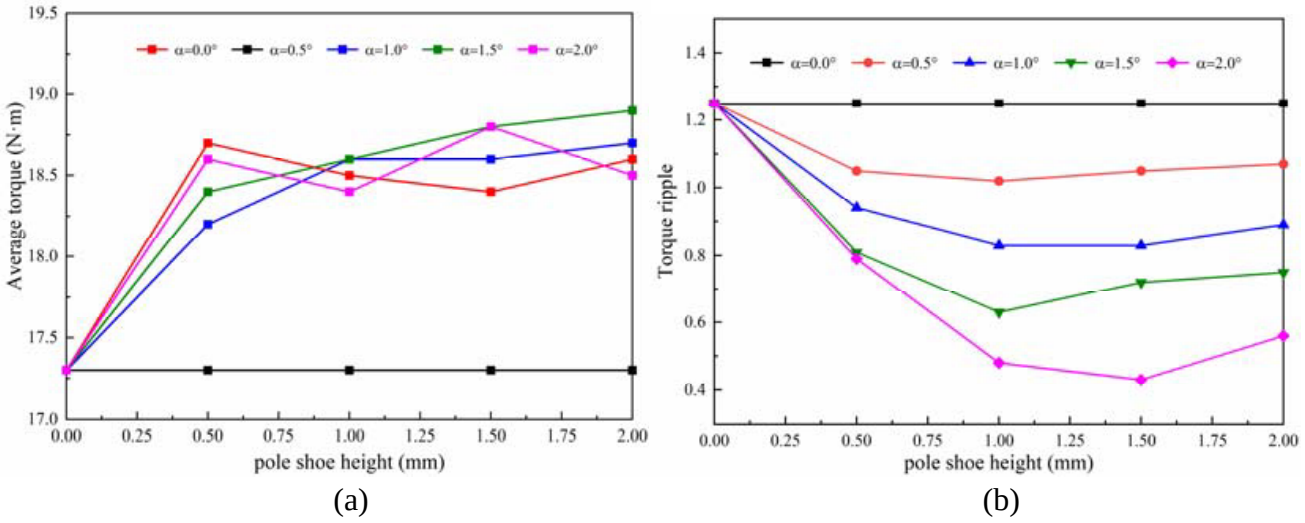

Figure 10. The torque characteristics of different pole shoe sizes. (a) Average torque, (b) torque ripple.

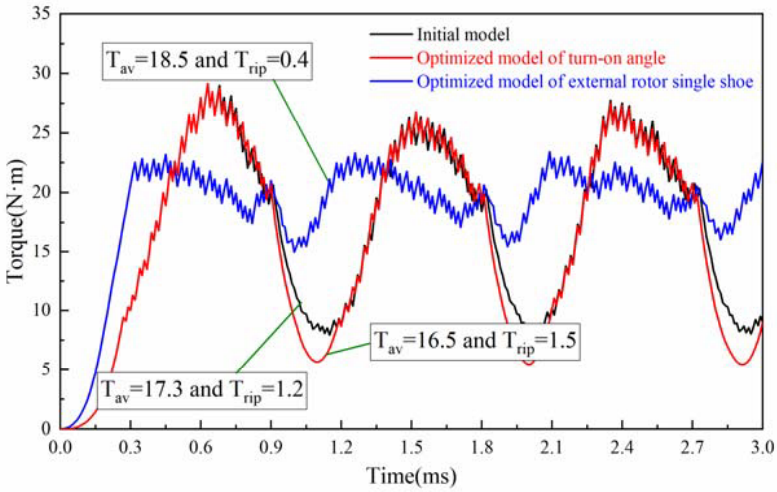

Figure 11. The torque comparison.

selected as the optimal height of pole shoe.

As shown in Fig. 11, the red curve represents the instantaneous torque of the initial model; the black curve represents the instantaneous torque when the model does not change, and the turn-on angle is $-1.5°$; the blue curve represents the instantaneous torque when the external rotor has single pole shoe, and turn-on angle is $-1.5°$. Comparing the torque characteristics of the optimized model and the initial model comprehensively, it is finally determined that the best turn-on angle is $-1.5°$, and the angle and height of single pole shoe are $2°$ and 1.5 mm, respectively, which reduces the torque ripple from 1.5 to 0.4 by 73.3% and greatly improves vibration of the machine.

5. VIBRATION ANALYSIS

5.1. Harmonic Response Analysis

The curve of amplitude-frequency characteristic of MTER-SRM can be obtained by Harmonic Response Analysis (HRA), such as vibration displacement, velocity, and acceleration of the stator components at

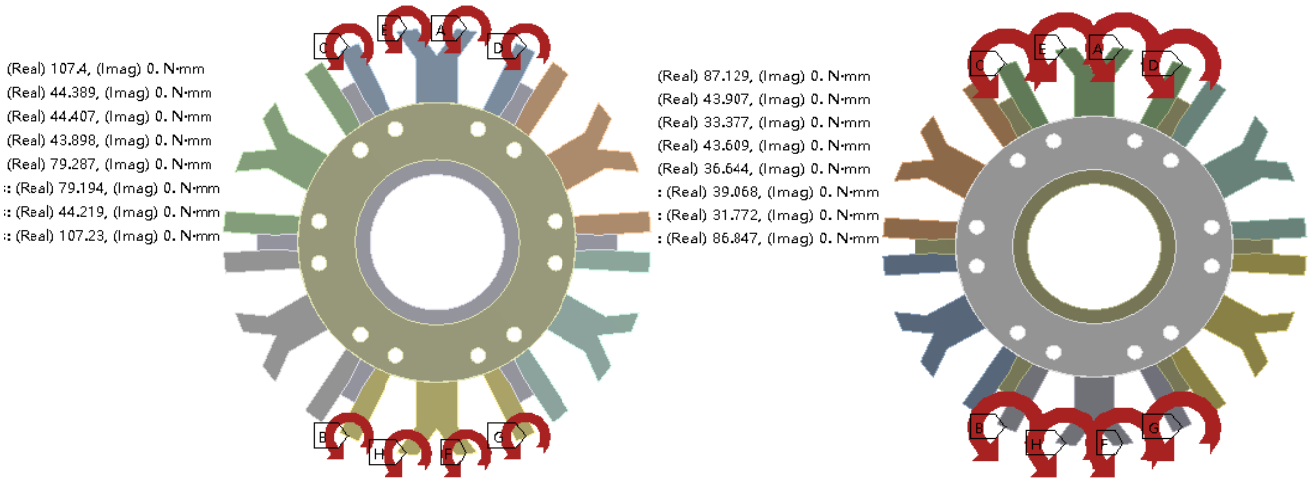

Figure 12. Torque component. (a) External rotor without single pole shoe, (b) external rotor with single pole shoe.

different frequencies. The stress situation can be obtained based on the maximum response point and peak frequency in the amplitude-frequency characteristic curve. The electromagnetic force of stator tooth calculated by Maxwell is imported into the model of the stator pole in the form of concentrated force. Figs. 12(a) and (b) show respectively the distributions of torque component in the model stator

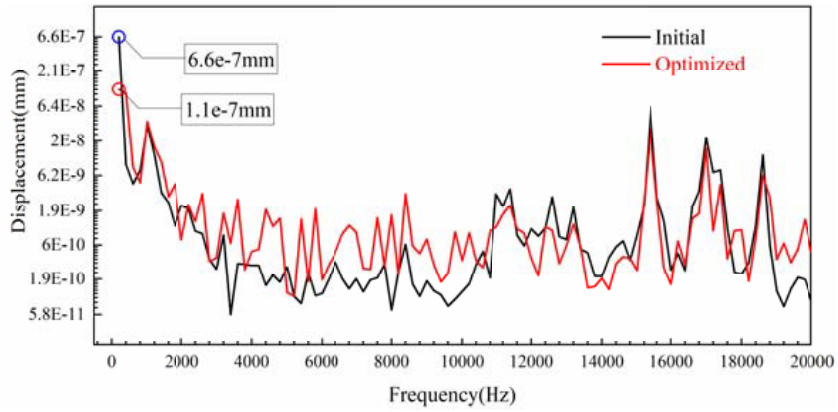

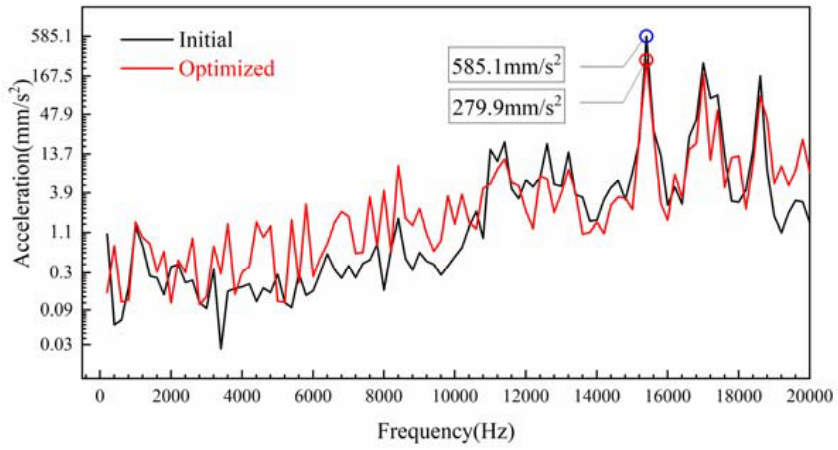

(c)

Figure 13. Comparison of vibration frequency response. (a) Vibration displacement, (b) vibration velocity, (c) vibration acceleration.

tooth before and after optimization.

The electromagnetic force of the stator teeth is calculated by Ansys-Maxwell in the last complete period; the data in the time domain will be converted into frequency domain with the frequency range of $0 \sim 1/(2\text{dT})$, and the vibration characteristics of the stator in the frequency range in $0 \sim 20$ MHz will be obtained.

The vibration displacement, velocity, and acceleration of the stator part before optimization are 6.6e-7 mm, 6.1e-3 mm/s, and 585.1 mm/s^2 before optimization in Fig. 13, respectively, which are 1.1e-7 mm, 2.9e-3 mm/s, and 279.9 mm/s^2 after optimization, reduce by 83.3%, 52.5%, and 52.2%, respectively. The vibration characteristics of the MTER-SRM are effectively improved.

5.2. Noise Analysis

Sound pressure is a physical parameter which describes the characteristics of the sound wave. The noise of motor mainly radiates along the radial direction of air. An air domain of 5 times the outer diameter of external rotor is established in the paper, as shown in Fig. 14.

Figure 14. The air domain.

The vibration velocity obtained is used as the excitation source of noise analysis, and it couples to the module of noise analysis to solve the air domain. The maximum sound pressure of the initial model is 2.4e-8MPa, as shown in Fig. 15, and that of the optimized model is 1.1e-8MPa, with decrease of 54.2%.

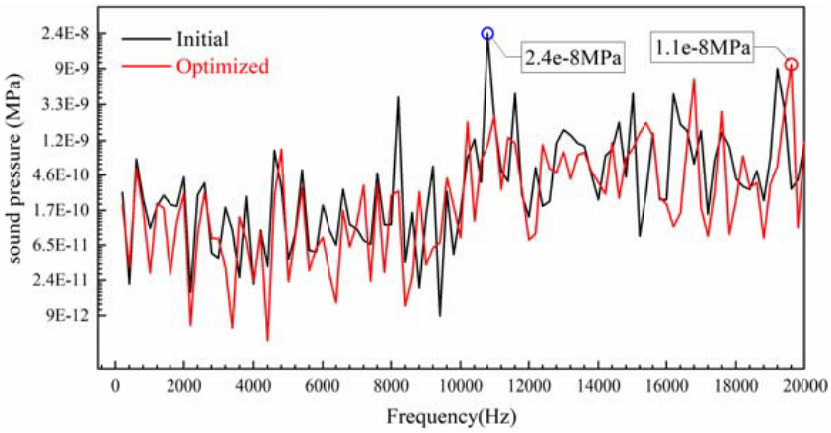

Figure 15. Noise pressure.

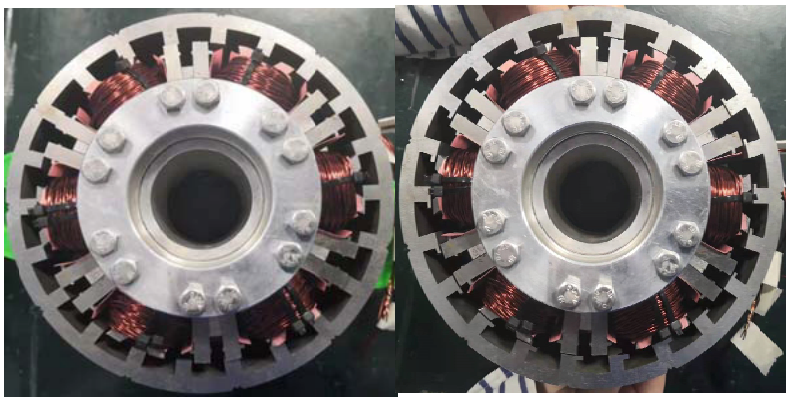

Figure 16. The two prototypes. (a) Initial model, (b) optimized model.

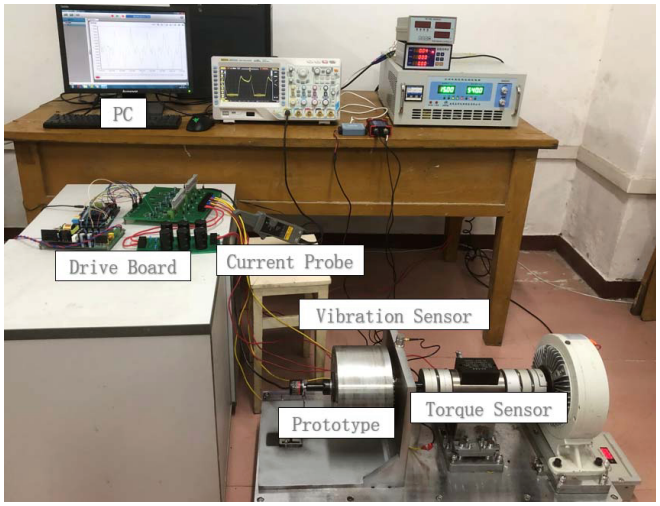

Figure 17. The test system.

6. PROTOTYPE EXPERIMENT

6.1. System of Prototype

The vibration test is important for measuring the parameter of vibration and noise to verify the effect of the simulation test. Two prototypes are made in Fig. 16, and the vibration test system is shown in Fig. 17. One is the initial model as in Table 1, and the other is an external rotor of optimized with the optimized size of pole shoe.

6.2. Prototype Experiment Results

The test speed is set at 1000 r/min, and vibration acceleration is shown in Fig. 18.

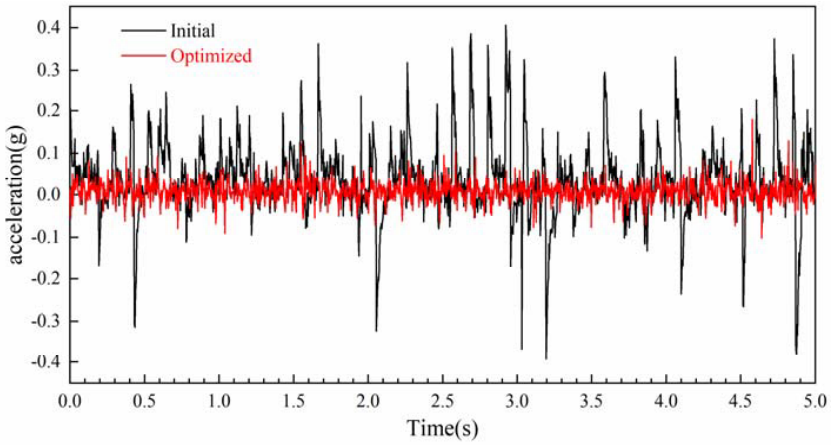

Figure 18. Vibration acceleration of prototype.

The maximum vibration accelerations of two models are 0.4 g and 0.1 g before and after optimization in Fig. 18, respectively, a reduction of 75%. The prototype experiment shows that the vibration and noise of the optimized model is significantly lower. The innovation proposed in this paper can easily suppress vibration and noise of other SRMs with an external rotor.

7. CONCLUSION

A new method by optimizing the turn-on angle and adding single pole shoe with an angle of 2° and height of 1.5 mm to the external rotor is proposed in the paper, by analyzing the causes of torque ripple and summarizing methods of restraining torque ripple. The theoretical analysis, electromagnetic simulation, and prototype experiment are carried out, and the following conclusions are made:

(1) The turn-on angle and pole shoe of external rotor has a great impact on the torque characteristics. The parameters of turn-on angle and size of pole shoe are obtained by FEM. Compared with the initial model, the torque ripple of the optimized model decreases from 1.2 to 0.4, with a decrease of 73.3%. It is effective to decrease the torque ripple.

(2) Multi-physical field simulation experiments shows that the vibration displacement, velocity, acceleration, and sound pressure of optimized model decrease by 83.3%, 52.5%, 52.2%, and 54.2%, respectively. The vibration test of the prototypes shows that the maximum vibration acceleration decreases from 0.4 to 0.1, with a decrease of 75%, which greatly decreases the vibration and noise of the motor. Optimizing turn-on angle and adding single pole shoe to external rotor can be used as reference about decreasing the vibration and noise suppression of other SRM with external rotor, which is low for manufacturing cost and easy to achieve it.

REFERENCES

1. Zhu, Z. Q., X. Liu, and Z. Pan, "Analytical model for predicting maximum reduction levels of vibration and noise in switched reluctance machine by active vibration cancellation," *IEEE Transactions on Energy Conversion*, Vol. 26, No. 1, 36–45, 2011.
2. Gan, C., J. Wu, Q. Sun, W. Kong, H. Li, and Y. Hu, "A review on machine topologies and control techniques for low-noise switched reluctance motors in electric vehicle applications," *IEEE Access*, Vol. 6, 31430–31443, 2018.
3. Takiguchi, M., H. Sugimoto, N. Kurihara, and A. Chiba, "Acoustic noise and vibration reduction of SRM by elimination of third harmonic component in sum of radial forces," *IEEE Transactions on Energy Conversion*, Vol. 30, No. 3, 883–891, 2015.
4. Qing, L. W. H. M. and X. L. Ge, "A high efficiency torque ripple suppression method for switched reluctance motor," *Transactions of China Electrotechnical Society*, Vol. 35, No. 9, 1912–1920, 2020.
5. Andrada, P., B. Blanqué, E. Martínez, and M. Torrent, "A novel type of hybrid reluctance motor drive," *IEEE Transactions on Industrial Electronics*, Vol. 61, No. 8, 4337–4345, 2014.
6. Jeong, K. I. X. Z. and D. H. Lee, "Performance comparison of conventional and segmental rotor type switched reluctance motor," *Journal of Electrical Engineering & Technology*, Vol. 13, No. 3, 1138–1146, 2018.
7. Mousavi-Aghdam, S. R., M. R. Feyzi, and Y. Ebrahimi, "A new switched reluctance motor design to reduce torque ripple using finite element fuzzy optimization," *Iranian Journal of Electrical & Electronic Engineering*, Vol. 8, No. 1, 91–96, 2012.
8. Gundogmus, O., M. Elamin, Y. Yasa, T. Husain, Y. Sozer, J. Kutz, J. Tylenda, and R. L. Wright, "Acoustic noise mitigation of switched reluctance machines with windows on stator and rotor pole shoes," *IEEE Transactions on Industry Applications*, Vol. 56, No. 4, 3719–3730, 2020.
9. Lee, D., T. H. Pham, and J. Ahn, "Design and operation characteristics of four-two pole shoe high-speed SRM for torque ripple reduction," *IEEE Transactions on Industrial Electronics*, Vol. 60, No. 9, 3637–3643, 2013.
10. Jiang, J. W., B. Bilgin, and A. Emadi, "Three-phase 24/16 switched reluctance machine for a hybrid electric powertrain," *IEEE Transactions on Transportation Electrification*, Vol. 3, No. 1, 76–85, 2017.
11. Huang, C. Z. S. W. F. and G. X. Guo, "Optimization of stator pole shoe shape based on torque ripple and radial force," *Electric Machines and Control*, Vol. 24, No. 6, 98–106, 2020.
12. Lee, J. H., "Optimum shape design solution of flux switching motor using response surface methodology and new type winding," *IEEE Transactions on Magnetics*, Vol. 48, No. 4, 1637–1640, 2012.
13. Yang, H., Y. Lim, and H. Kim, "Acoustic noise/vibration reduction of a single-phase SRM using skewed stator and rotor," *IEEE Transactions on Industrial Electronics*, Vol. 60, No. 10, 4292–4300, 2013.
14. Nabeta, S. I., I. E. Chabu, L. Lebensztajn, D. A. P. Correa, W. M. D. Silva, and K. Hameyer, "Mitigation of the torque ripple of a switched reluctance motor through a multiobjective optimization," *IEEE Transactions on Magnetics*, Vol. 44, No. 6, 1018–1021, 2008.
15. Guo, X., R. Zhong, M. Zhang, D. Ding, and W. Sun, "Resonance reduction by optimal switch angle selection in switched reluctance motor," *IEEE Transactions on Industrial Electronics*, Vol. 67, No. 3, 1867–1877, 2020.
16. Li, G., J. Ojeda, S. Hlioui, E. Hoang, M. Lecrivain, and M. Gabsi, "Modification in rotor pole shoe geometry of mutually coupled switched reluctance machine for torque ripple mitigating," *IEEE Transactions on Magnetics*, Vol. 48, No. 6, 2025–2034, 2012.
17. Lee, J. W., H. S. Kim, B. I. Kwon, and B. T. Kim, "New rotor shape design for minimum torque ripple of SRM using FEM," *IEEE Transactions on Magnetics*, Vol. 40, No. 2, 754–757, 2004.
18. Zhang, X., X. Wang, and Y. Yang, "The computation of vibration reduction capacity for switched reluctance motor based on improved magnetic field partition method," *Transactions of China Electrotechnical Society*, Vol. 30, No. 22, 9–18, 2015.

19. Zhang, X., X. Wang, Y. Yang, and B. Wei, "Vibration reduction of a switched reluctance motor using new rotor tooth with slot on each side," *Proceedings of the CSEE*, Vol. 35, No. 6, 1508–1515, 2015.
20. Lin, F. and S. Yang, "An approach to producing controlled radial force in a switched reluctance motor," *IEEE Transactions on Industrial Electronics*, Vol. 54, No. 4, 2137–2146, 2007.
21. Mousavi-Aghdam, S. R., M. R. Feyzi, N. Bianchi, and M. Morandin, "Design and analysis of a novel high-torque stator-segmented SRM," *IEEE Transactions on Industrial Electronics*, Vol. 63, No. 3, 1458–1466, 2016.